Study of charged soot aggregates formed by benzene pyrolysis.

N. A. Ivanova, A. M. Baklanov, V. V. Karasev, A. A. Onischuk

Institute of Chemical Kinetics and Combustion, Russian Academy of Sciences, Novosibirsk, 630090, Russia

Soot formation during benzene pyrolysis is of interest due to use of fuels with increased aromatic content resulting in high level of particulate emissions from vehicular exhausts, furnaces, and manufacturing processes relatively to those emissions from low C/H ratio fuels. This work is aimed at video system investigation of charged soot aggregate formation due to benzene pyrolysis in reactor presented in Fig. 1. A mixture of benzene with nitrogen is supplied to the input of reactor at
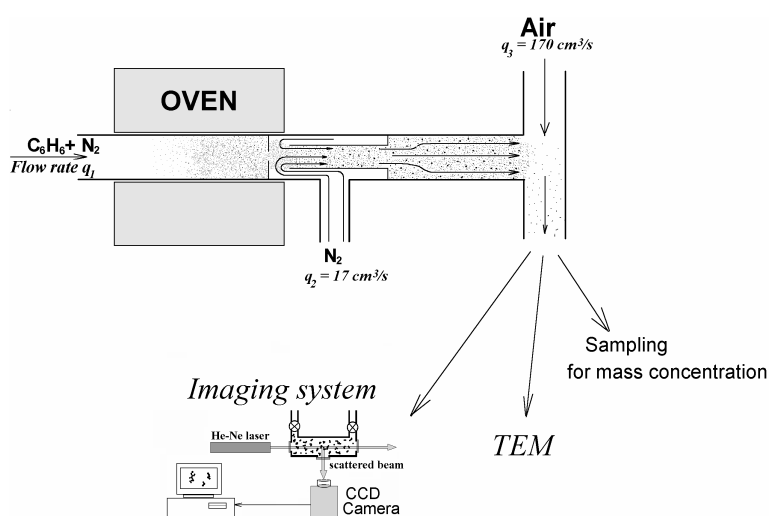

Fig. 1. Scheme of the experimental set-up.

atmospheric pressure and room temperature. The partial pressure of benzene in this mixture is 100 Torr. The experiments were carried out at the temperature in reaction zone of 1350 K. The input flow rate is varied in the range $q_1 = 0.25 - 2.5$ scc/s which corresponds to the residence time in reaction zone $t = 0.6 - 6$ c. The pyrolysis of

Fig. 2. Example of TEM image of soot aggregates

benzene resulted in soot aggregate formation (Fig. 2). The size of aggregates is 0.1 - 1 μm, the mean size of primary particles about 100 nm. Using the TEM images the

average radius of aggregates was measured as a function of the height above burner. The radius was determined as:

$$R = \frac{1}{2}\sqrt{LW} \qquad (1)$$

where L and W are the dimensions of the rectangle enclosing the image of single particles or aggregate. Fig. 3a shows frequency distribution of aggregate radius.
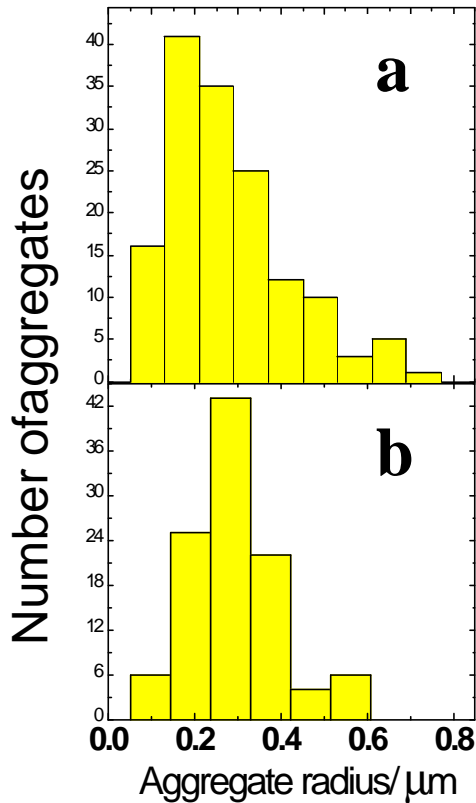

Fig. 3. Frequency distribution of aggregate radius; a) TEM data; b) Video observations. Input flow rate $q_1 = 0.8$ cm^3/c.

We described the aggregate morphology in terms of fractal-like dimension D_f which can be determined from a power relation between the mass M of each aggregate and its radius R measured by TEM analysis:

$$M \propto R^{D_f} . \qquad (2)$$

To determine D_f the values of aggregate masses were plotted as $logM$ vs. $logR$ (Fig. 4). To determine the aggregate mass (in arbitrary units) we measured the "integral
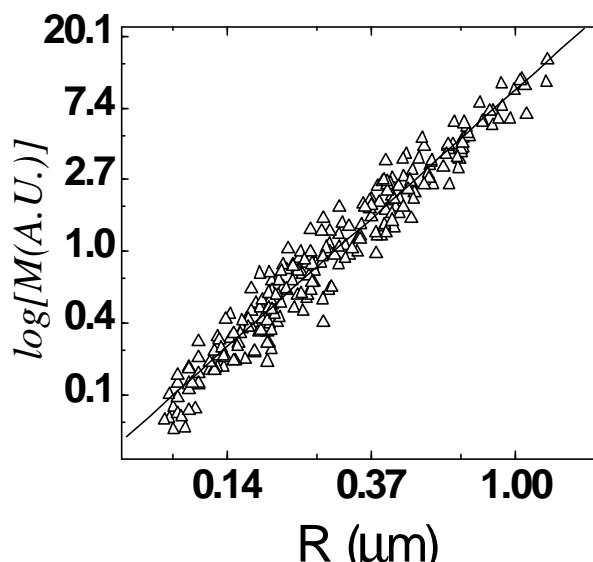

Fig. 4. Soot aggregate mass vs. radius. TEM data. Solid line corresponds to $D_f = 1.7$.

optical density" of individual aggregate TEM image. It is assumed that the local optical density in the aggregate image is proportional to the local aggregate thickness. As follows form Fig. 4 $D_f = 1.7$.

An imaging system was used for soot observations. To this aim, a small portion of aerosol was injected to an optical cell. Light of a He-Ne laser beam scattered by soot particles at an angle of 90° passed through a flat window to a microscope objective and then to a CCD camera connected to a TV system. This optical set-up resolves images of aggregates larger than about 3 μm; smaller aggregates were visible as spots. To create an electric field, two parallel electrodes were fixed in the cell at a distance of 0.25 cm. The velocity of aggregate movement in the electric field with intensity of 360 V/cm gave information on the electric charge of aggregates. We estimated the aggregate net charge from the balance between the Coulomb force and the drag force. The crucial point in these estimations was determination of equivalent radius of aggregate R_m. Two different approaches were applied. In the first approach the mobility equivalent radius of each aggregate was derived from the observation of it's Brownian motion without electric field. An example of the aggregate trajectory observed by the video system is presented in Fig. 5. The aggregate diffusion
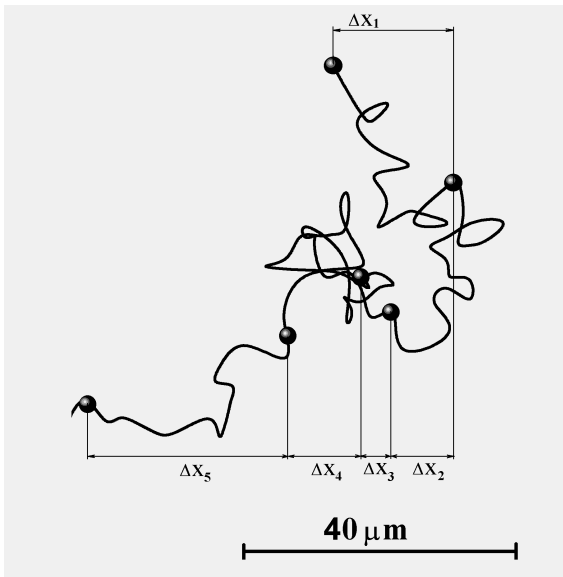

Fig. 5. Example of the aggregate trajectory registered by the video system.

coefficient D was determined from the Einstein equation: $\overline{(\Delta x)^2} = 2Dt$,

$\overline{(\Delta x)^2} = \dfrac{\Delta x_1^2 + \Delta x_2^2 + ... + \Delta x_n^2}{n}$; where $\Delta x_1, \Delta x_2, ..., \Delta x_n$ are successive displacements of the aggregate along horizontal x-axis over time interval t (see Fig. 5). Then the effective radius was derived from the diffusion coefficient. Fig. 3b demonstrates frequency distribution of effective mobility radius determined by video observation of aggregate Brownian motion. After recording of the aggregate Brownian motion the electric field was switched on to measure the velocity of aggregate movement due to electric force (Fig. 6). This approach resulted in charge distribution over aggregates presented in Fig. 7a. In the second approach the same average mobility radius was used to characterise each aggregate recorded by the video system. This average R_m was determined by elaboration of TEM images assuming equivalence of the mean mobility radius R_m and mean projected area radius R_a . Figure 6b shows frequency distribution of aggregate charge for the second way of data treatment. One can see from Figs 3, 7 a good agreement between two approaches in estimation of aggregate size and charge distribution.
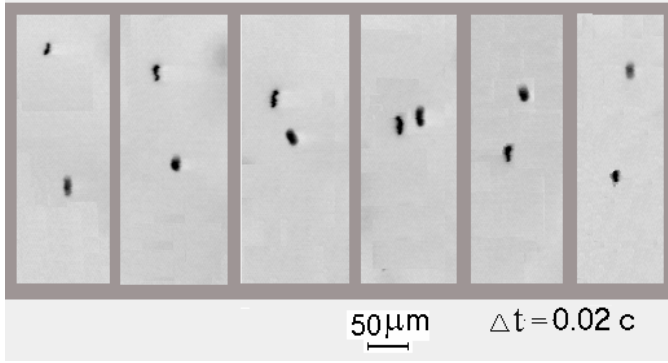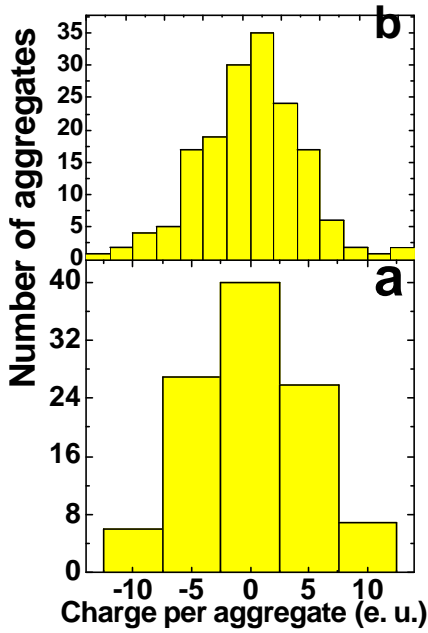
Fig. 6. Video frames demonstrating the aggregate movement in homogeneous electric field (360 V/cm). Time increases from left to right.

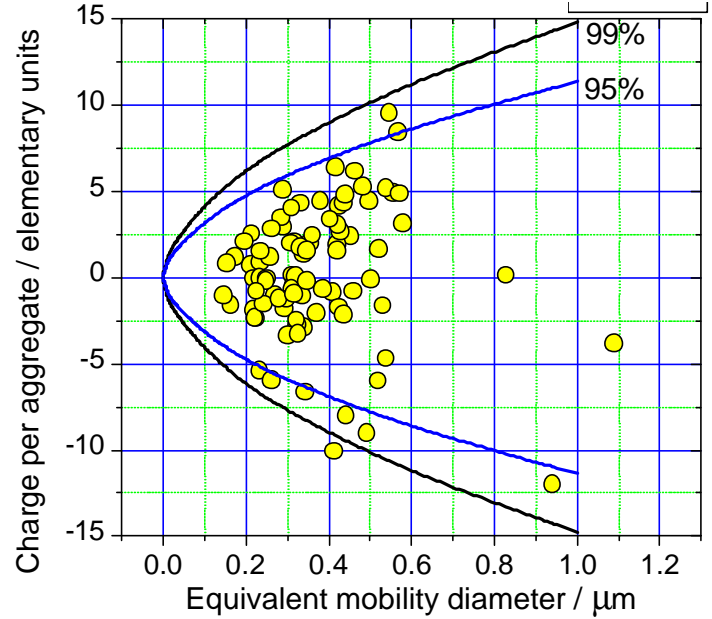???. 7. Frequency distribution of aggregate charge. a) Video observation data; b) TEM data. Input flow rate $q_1 = 0.8$ cm^3/c.

Fig. 8. Size - charge distribution of soot aggregates formed at input flow rate $q_1 = 0.25$ cm^3/s. Solid lines cover 95 and 99% probability regions for stationary distribution governed by equations (3, 4)

After long enough coagulation an ensemble of charged particles will reach a stationary charge and size distribution. Thus, for example, if coagulation is accompanied by a generation of bipolar ions, the stationary charge distribution of aerosol is governed by the Bolzmann formula [1]:

$$f(n) = \frac{1}{\Sigma} \exp\left(-\frac{q^2}{2RkT}\right) \tag{3}$$

$$\Sigma = \sum_{-\infty}^{\infty} \exp\left(-\frac{(q)^2}{2RkT}\right) \tag{4}$$

where R is radius of particles, q is particle charge, k is Boltzmann constant, T is temperature. Fig. 8 demonstrates charge - radius frequency distribution of soot aggregates sampled for the inlet flow rate of 0.25 cm^3/s. Solid lined covers fields of 95 and 99% probability for stationary distribution governed by Eqs. (3) and (4). From the
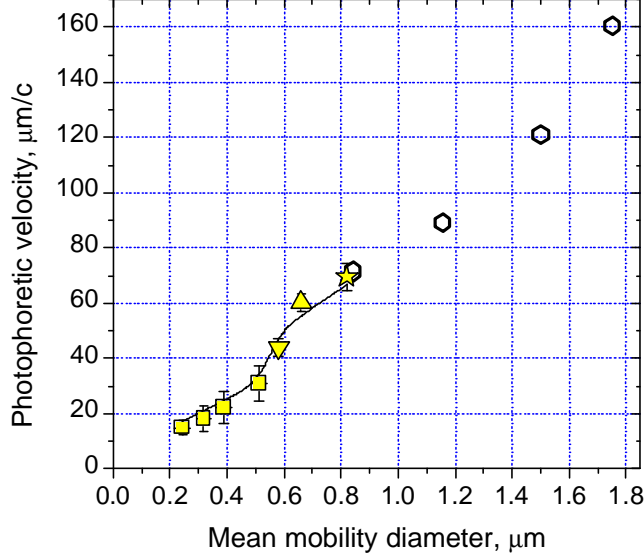
Fig. 9. Photophoretic velocity vs. mobility equivalent diameter of aggregates. Solid symbols - direct video registration, input flow rate q = 0.25 (■); 0.8 (▼); 1.4 (▲); 2.5 cm³/s (★). Open symbols - sedimentation data (Fig. 10). Line - estimation based on Eqs. 5, 6.
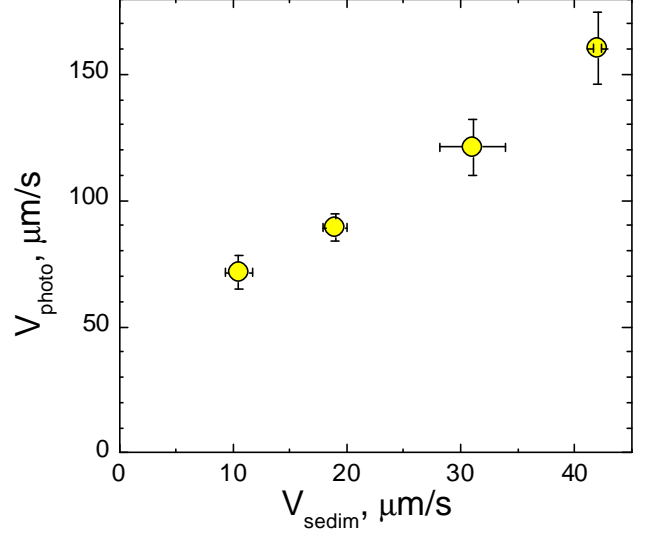
Fig. 10. Photophoretic velocity vs. sedimentation velocity for soot aggregates.

comparison between experimental data and estimation results presented in Fig. 8 we assume that charge distribution corresponds to stationary conditions.

Photophoresis of soot aggregates driven by helium-neon laser beam was studied using the video system. Fig. 9 (solid symbols) illustrates the photophoretic velocity vs. equivalent mobility diameter of aggregates (determined by video observation of Brownian movement of aggregates). To explain the observed photophoretic velocity increase with aggregate diameter we estimated the photophoretic force as [1]:

$$F_{ph} = -\frac{ph\sqrt{\dfrac{R}{MT}}\Gamma_i}{\dfrac{P}{P_0} + \dfrac{P_0}{P}} R_a^{\ 2} \qquad (5)$$

where h is viscosity coefficient, R is gas constant, M is mass of gas molecules, G_i is temperature gradient inside of the particle, P is ambient gas pressure,

$$P_0 = \frac{3h}{r}\sqrt{\frac{RT}{M}}, \qquad (6)$$

where r is radius of primary particles in aggregate. Photophoretic velocity was determined from the balance between F_{ph} and the drag force. Figure 9 demonstrates a reasonable agreement between experimental data and estimation.

Some aggregates observed by video system were large enough to sedimentate in the gravity of Earth. We observed both sedimentation and photophoretic movement for the same aggregates. Fig. 10 shows photophoretic velocity V_{photo} vs. sedimentation velocity V_{sedim}. Each point in the graph was determined by averaging over large number of original points V_{photo} - V_{sedim} for single aggregates. One can see from Fig. 10 that the photophoretic velocity increases together with sedimentation velocity. In

other words, the larger is the size of aggregates the higher is the photophoretic velocity. It seems to be interesting to compare the data of Fig. 10 with photophoretic velocity data presented in Fig. 9 vs. equivalent mobility diameter. To adjust the sedimentation - photophoretic data to the photophoretic velocity - equivalent mobility diameter results (Fig. 9) we assume that the point with the lowest photophoretic velocity 71.5 µm/s in Fig. 10 corresponds to the equivalent mobility radius $R_m = 0.42$ µm. Thus from the balance between drag force and gravity force we have:

$$\frac{6\pi v_{sedim} \eta R_m}{(1+\frac{lA}{R_m})} = \frac{4}{3}\pi R_m^3 \rho_{eff} g \tag{7}$$

where ρ_{eff} is equivalent density of aggregates, g is gravity acceleration, l is the gas mean free path, A is the Cunningham correction factor ($A = 1.26$)..Thus, from $v_{sedim}=$ 10.5 µm/s and $R_m = 0.42$ we have $\rho_{eff} = 0.42$ g/cm^3. Using this equivalent density we can estimate equivalent mobility radius from the sedimentation velocity for the other points of Fig. 10. These estimation results are presented in Fig. 9 as open hexagons. One can see a reasonable agreement between the sedimentation data and Brownian movement data.

<div align="center">References</div>

1. Fuchs N. A. *The mechanics of aerosols*; Pergamon Press: Oxford, 1964.